

Steam Effects on the Oxidation Behaviour of Al₂O₃-Scale Forming Ni-Based Alloys

Wei Zhao · Brian Gleeson

Received: 16 April 2012 / Published online: 19 January 2013
© Springer Science+Business Media New York 2013

Abstract The effects of steam on the 1,000 °C oxidation behavior of Al₂O₃-scale forming Ni-based alloys were studied by conducting tests in dry air and air + 30 % steam (wet air) gas environments. It was found that the critical concentration of Al (N_{Al}^*) to form a continuous alumina scale is increased when the environment is wet air. From the morphology of and the depth at which the internal oxides formed in the two oxidizing conditions, it was determined that the enrichment factor α remained the same in dry and wet air, though the internal-oxide precipitates were coarser and their average spacing greater in the wet air. Based on an assessment of the parameters contained in Wagner's criterion for transition from internal oxidation to external scale formation, it was deduced that the only factor that can change the critical concentration N_{Al}^* to the extent measured is the critical volume fraction f_v^* .

Keywords Steam effect · Oxidation map · Ni-based alloy · Critical concentration of Al

Introduction

Nickel-based super alloys are used extensively at elevated temperatures due to their good oxidation and corrosion resistance [1]. The protection of an alloy typically relies on its ability to form a continuous Al₂O₃ or Cr₂O₃ scale during thermal exposure. The design of Ni-based superalloy compositions is usually based on the Ni–Cr–Al system with other elements added primarily for strength [2, 3]. Therefore,

W. Zhao (✉) · B. Gleeson
Department of Mechanical Engineering and Materials Science, University of Pittsburgh, 3700
O'Hara Street, 15260 Pittsburgh, PA, US
e-mail: wez29@pitt.edu

B. Gleeson
e-mail: bgleeson@pitt.edu

a good understanding of the oxidation behavior of the Ni–Cr–Al system is very helpful from the standpoint of alloy design.

The Ni–Cr–Al system has been widely studied under a variety of test conditions [2–7]. Among those studies, Giggins and Pettit [2] investigated the oxidation behavior of Ni–Cr–Al alloys in 0.1 atm oxygen at 1,000–1,200 °C. From their seminal study, three trends in oxidation behavior were identified and qualitatively summarized on an oxidation map. Figure 1 shows a typical oxidation map at 1,000 °C for Ni–Cr–Al alloys exposed to a dry oxidizing condition. The three trends or regions on the map correspond to NiO-scale forming, Al₂O₃-scale forming and Cr₂O₃-scale forming. The boundary between the NiO- and Al₂O₃-scale forming regions is important, since it defines the lowest Al concentration (N_{Al}^*) in an Ni–Cr–Al alloy required to form a continuous Al₂O₃ scale. This critical concentration is dictated by a variety of thermodynamic and kinetic factors associated with the alloy and the environment [8–13]. Values of N_{Al}^* can be estimated on the basis of two criteria proposed by Wagner [14, 15]. In one criterion [14], N_{Al}^* represents the minimum Al concentration for the transition from Al₂O₃ forming as internal precipitates to forming as an external scale. In the other criterion [15], for which a continuous Al₂O₃ scale is assumed to be already present, N_{Al}^* gives minimum supply of Al from the alloy to the alloy/scale interface necessary to sustain the Al₂O₃-scale growth. These two criteria have been tested for Ni–Al binary alloys oxidized in dry oxygen (0.1 atm) at 1,200 °C [8]. It was found that the criterion for the transition from internal to external oxidation was in best agreement with the experimental results.

To date, published oxide maps for the Ni–Cr–Al system are based on oxygen being the only oxidant in the gas atmosphere. However, considerable recent

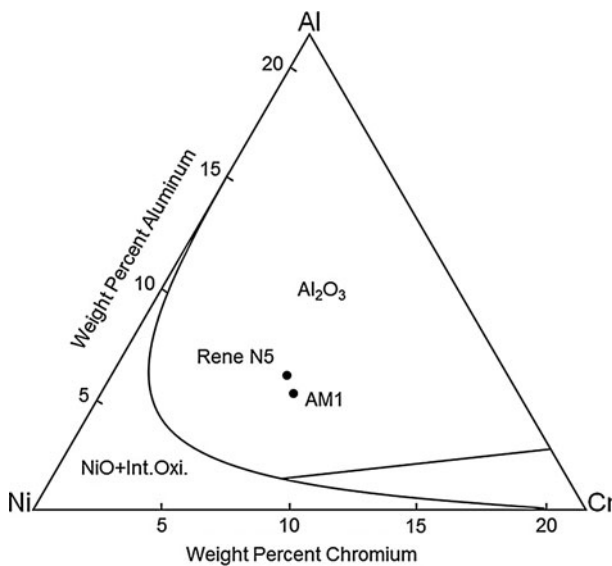


Fig. 1 Oxidation map for rolled Ni–Cr–Al alloy in 0.1 atm oxygen at 1,000 °C (based on ref. 2)

attention has been paid to the presence of steam in the atmosphere and the consequential effect(s) of steam on the oxidation behavior. Indeed, new combustion processes to increase the efficiency as well as to reduce the carbon dioxide emission tend to have relatively high steam contents, e.g., up to 80 % for a potential oxy-fuel combustion process [16]. Steam has been found to be detrimental to the oxidation of metals and alloys in a variety of ways [4, 5, 17–19]. For example, the scaling rate of Fe can be increased by a factor of 1.6 in the presence of steam [20]. It was also found that steam promotes the breakaway oxidation of some Cr₂O₃-scale forming Fe-based alloys, i.e., an alloy which can form a protective scale in a dry oxidizing condition becomes non-protective by the presence of steam [21]. This means that the critical concentration to form a protective scale is increased in wet oxidizing conditions. It has been proposed by some that this increase in N_{Cr}^* may be due to the enhanced Cr depletion as a consequence of volatile CrO₂(OH)₂ formation [22, 23]. Alternatively, Essuman et al. [17] speculated that N_{Cr}^* is increased in the presence of steam due to enhanced oxygen permeability into the alloy. However, no specific measurements were made to substantiate this speculation.

The proposed mechanisms discussed above are for Cr₂O₃-scale forming Fe-based alloys and they may not be valid for other alloy systems. In the past, some research has been carried out to determine the effects of steam on Al₂O₃-scale forming Ni-based alloys; although, those studies focused primarily on commercial alloys, which contain a variety of alloying elements. Such highly alloyed systems bring much complexity to clearly ascertaining the fundamental oxidation mechanism(s) associated with the steam effects. Therefore, a thorough study using model alloy systems is needed. Further, a quantitative analysis is needed to determine the key reason(s) for any shift in N_{Al}^* for an Al₂O₃-scale forming Ni-based system. The results presented here are from a more detailed study on the effects of steam on the oxidation behavior of model and commercial Ni-based alloys [24].

Experimental Procedures

Small ingots of two Ni–Cr–Al model alloys of nominal compositions given in Table 1 were prepared by Ar arc-melting followed by drop-casting to form 25 mm diameter rods. These alloys were cut into 5 mm thick disks and then given a preliminary annealing in vacuum at 1,000 °C for 48 h. Each disk was cold rolled to about 1 mm thickness and then annealed in vacuum at 1,000 °C for 48 h to promote homogeneity. The commercial alloys Rene N5 and AM1, with nominal compositions also given in Table 1, were cut from their as-received 2 mm-thick sheets into 10 × 10 × 2 mm test coupons. All samples were polished to a 600-grit finish and then ultrasonically cleaned in acetone immediately before oxidation testing. Air with a steam content of less than 2 ppm was used for the dry oxidation tests, while air + 30 %H₂O was produced by bubbling air through a water bath at 72 °C to saturate the air with steam and then through a condenser at 69 °C ($P_{H_2O} = 0.3$ atm) to remove the excess steam.

Table 1 Nominal composition (wt%) of model alloys and commercial superalloys AM1 and Rene N5

Alloy	Ni	Cr	Al	Co	Mo	W	Ta	Ti	Hf	Y	B	C	Re
Model #1	Bal	9.2	2.4										
Model #2	Bal	4.6	2.4										
Rene N5	Bal	7	6.2	8	2	5	6	0	0.2	0.01	0.004	0.05	3
AM1	Bal	7.5	5.3	6.5	2	5.5	8	1.2	0	0	0	0	0

Isothermal oxidation tests were done in both dry and wet conditions at 1,000 °C. After switching from tests in dry air to tests in wet air, the mixture of air + 30 %H₂O was first flowed through the whole system for 24 h to ensure that all the excess air was removed. A given test consisted of heating the furnace to 1,000 °C while the test samples were in the cold zone of the system, stabilizing the test atmosphere by flowing air + 30 %H₂O through the system for two hours, and then pushing the samples into the hot zone and holding them there for a pre-determined reaction period. At the completion of testing the samples were pulled from the hot zone and allowed to cool before being removed from the system.

The oxidized samples were prepared using standard metallographic preparation techniques. Cross-sections of the reacted samples were analyzed by scanning-electron microscopy (SEM), which was equipped with an energy-dispersive X-ray spectrometer (EDS) to allow for chemical analysis.

Results and Discussions

Figure 2 shows cross-sectional SEM images of AM1 and Rene N5 after oxidation in dry air and air + 30 %H₂O (wet air) at 1,000 °C for 20 h. Since these images were taken from back-scattered electrons (BSE), phases with a higher average atomic number appear brighter. The AM1 oxidized in dry air (Fig. 2a) formed an outer scale that was identified to be Ni(Cr,Al)₂O₄ via compositional analysis using EDS. This layer contained a discrete band of white particles which were inferred to be oxides rich in tungsten and tantalum. Below the spinel layer, there was a continuous Al₂O₃ layer in the contact with the base alloy. By contrast, when this alloy was oxidized in wet air (Fig. 2b), it did not form a continuous Al₂O₃ scale. Instead, it formed an outermost region comprised of NiO and Ni(Cr,Al)₂O₄ spinel. Al₂O₃ formed only as discrete internal oxide protrusions. Therefore, steam was detrimental to the 1,000 °C oxidation behavior of this alloy by inhibiting the formation of a continuous Al₂O₃ scale. As shown in Fig. 2, however, the Rene N5 was not as vulnerable to the presence of 30 % steam. This alloy formed a uniform and continuous Al₂O₃ scale in both dry (Fig. 2c) and wet air (Fig. 2d) at 1,000 °C. Even so, when the Rene N5 was oxidized in wet air, a distinct spinel layer formed above the Al₂O₃ scale. The spinel layer is believed to be a consequence of NiO formation during the early stages of oxidation which, in turn, indicates that the establishment of a continuous Al₂O₃ scale layer was slower in wet air than in dry.

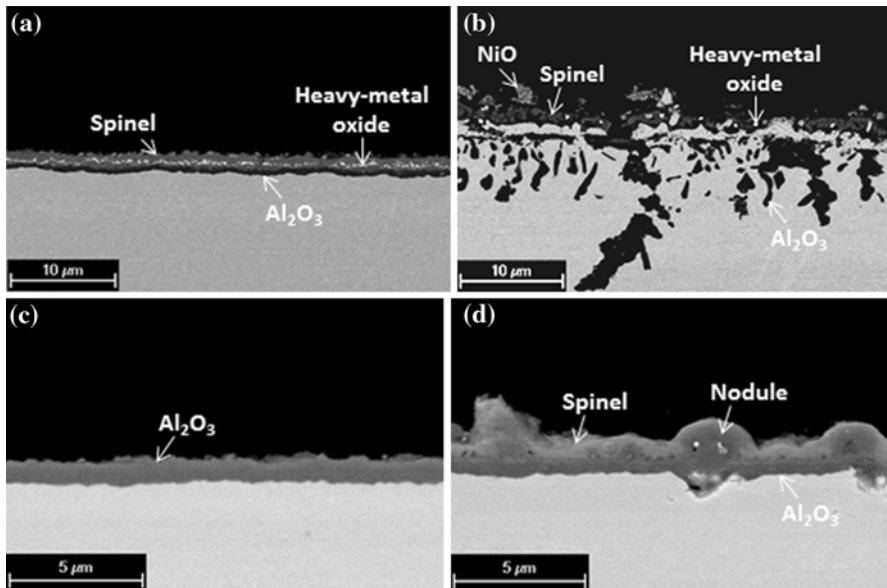


Fig. 2 Cross-sectional BSE images of commercial alloy AM1 (a, b) and Rene N5 (c, d) oxidized in dry air (a, c) and air + 30 %H₂O (b, d) at 1,000 °C for 20 h

Comparing the compositions in Table 1, it is seen that AM1 has a lower Al content (5.3 wt% compared to 6.2 wt%) but a slightly higher Cr content (7.5 wt% compared to 7 wt%) than Rene N5. The combination of the Al and Cr concentrations, as well as some other added elements, caused AM1 to have only marginal ability to form a protective Al₂O₃ scale in dry air at 1,000 °C and to become less protective when it was oxidized in wet air. However, it is not easy to draw a conclusion whether the better oxidation behavior of Rene N5 was due to its slightly higher Al concentration or due to some other compositional and/or structural factors. To better elucidate the effect of steam on the oxidation behavior of Al₂O₃-scale forming Ni-based alloys, a more detailed analysis was conducted on Ni–Cr–Al model alloys.

Figure 3 shows the oxidation behavior of the model alloy 1 (Ni-9.2Cr-2.4Al) in dry and wet air at 1,000 °C for 20 h. In dry air (Fig. 3a), a continuous Al₂O₃ scale formed, indicating this alloy is protective at this temperature. However, this alloy became less protective when oxidized in wet air (Fig. 3b). In this latter case, an NiO scale formed on the surface, followed by an intermediate layer of the Ni(Cr,Al)₂O₄ spinel and then discrete internal oxidation precipitates within the alloy. Clearly, the concentrations of Al and Cr in this model alloy were not sufficient to form a continuous Al₂O₃ scale in the wet oxidizing condition. Stated differently, N_{Al}^* is increased under the wet oxidizing conditions studied here. In fact, it was found that N_{Al}^* increased by 60 % [24]. Such a substantial increase in N_{Al}^* is assessed in the following by considering Wagner's two criteria [14, 15]. As a starting point, it is essential to determine which criterion is applicable for this situation.

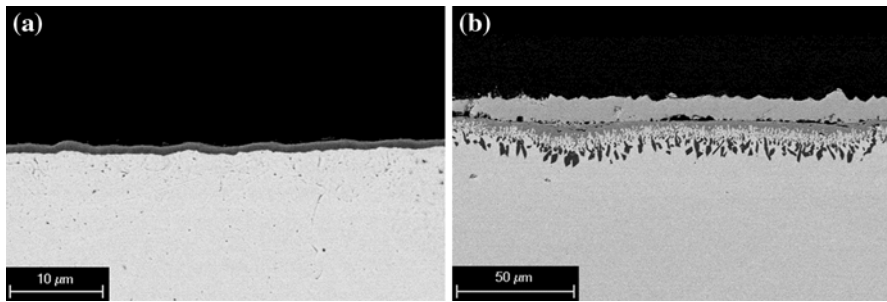


Fig. 3 Oxidation behavior of Ni-9.2Cr-2.4Al in dry (a) and wet (b) air at 1,000 °C for 20 h

In Wagner's criterion [15] for sustaining the growth of a continuous Al_2O_3 scale, the minimum amount of Al in the alloy (N_{Al}^*) to sustain the growth of a continuous external Al_2O_3 scale is found to be:

$$N_{\text{Al}}^* \geq \frac{V_{\text{all}}}{vM_{\text{O}}} \left(\frac{\pi \cdot k_p}{2D_{\text{Al}}} \right)^{1/2} \quad (1)$$

where V_{all} is the molar volume of the alloy, v the stoichiometry factor for AlO_x , M_{O} the atomic weight of oxygen, k_p the growth rate constant of the Al_2O_3 scale in the units of $\text{g}^2/\text{cm}^4 \text{ sec}$ and D_{Al} the diffusion coefficient of aluminum in the alloy. This equation indicates that when there is a protective Al_2O_3 scale formed initially, an enhanced growth rate of this scale (k_p) in the presence of steam will increase the consumption of Al and, therefore, increase N_{Al}^* . For the criterion based on Eq. 1 to be applicable, a continuous Al_2O_3 scale has to form initially. Specific to this model alloy, it is necessary to clarify whether the different oxidation behaviors observed at 20 h (Fig. 3) existed from the very early stages of oxidation or if there was an initial stage in which this alloy formed a continuous Al_2O_3 scale in both atmospheres but the Al_2O_3 scale eventually broke down in air + 30 % H_2O . Figure 4 compares the surface morphology of model alloy 1 oxidized in dry air (a, b) and in air + 30 % H_2O (c, d) at 1,000 °C for 5 min (a, c) and 30 min (b, d). It is seen that the difference in the oxidation behaviors of this alloy in the two environments existed from the initial stages of oxidation: when the alloy was oxidized in dry air, only Al_2O_3 formed at 5 min (dark gray area in Fig. 4a) and the Al_2O_3 became continuous before 30 min (Fig. 4b). By contrast, when this alloy was oxidized in air + 30 % H_2O , NiO initially formed as discrete islands (Fig. 4c) and then became continuous with time (Fig. 4d). Therefore, it is clear that Wagner's criterion for sustaining the external Al_2O_3 scale is not applicable to accounting for the increased N_{Al}^* of this alloy when steam is present.

In accordance with studies on Fe-based Cr_2O_3 -scale forming alloys [17], the observed shift in N_{Al}^* when steam is present in the atmosphere may possibly be explained by an increase in the oxygen permeability into the alloy. This hypothesis is based on a limiting condition of Wagner's criterion for the transition from internal oxidation to external scale formation [25], i.e.,

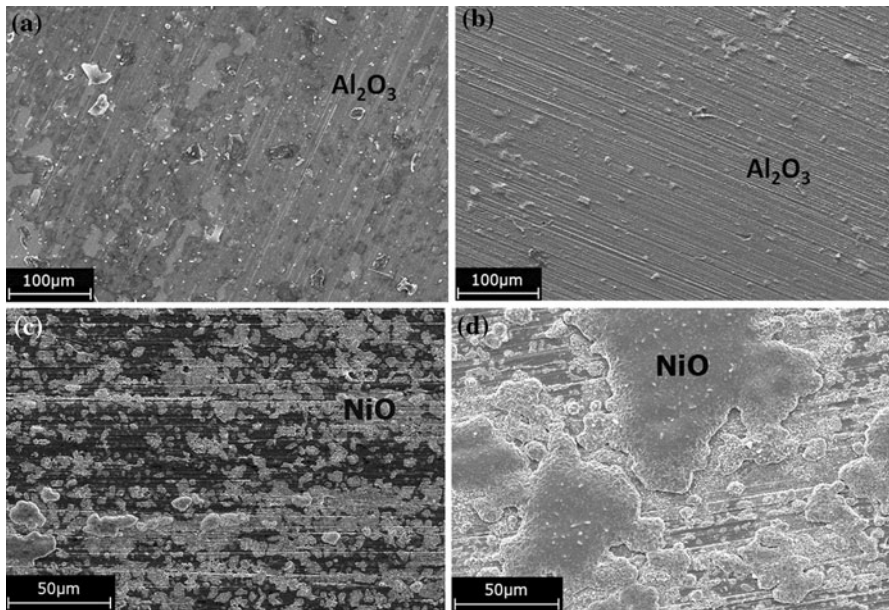


Fig. 4 Comparison of steam effect on Ni-9.2Cr-2.4Al oxidized in dry air for **a** 5 min **b** 30 min and in air + 30 %H₂O for **c** 5 min and **d** 30 min. In **(a)** and **(b)**, the dark area are Al₂O₃ scale

$$N_{Al}^* \propto \left(\frac{N_o^S D_o}{D_{Al}} \right)^{1/2} \tag{2}$$

where N_o^S is the concentration of dissolved oxygen at the alloy surface and D_o is the diffusion coefficient of oxygen in the alloy. The product of N_o^S and D_o defines the oxygen permeability into the alloy. As shown by Eq. 2, if this parameter is enhanced, the value of N_{Al}^* will increase. To assess oxygen permeability in our case, the internal oxidation behavior of a dilute Ni–Al alloy in wet and dry oxidizing conditions was compared. Since the oxygen partial pressure in air is high enough to oxide nickel, the internal oxidation is coupled with external NiO formation. Therefore, the oxygen permeability needed to be calculated by Maak’s modification [26] as:

$$N_o^S D_o = v N_{Al}^O \frac{\xi_i (\xi_i - \xi_c)}{2t} \left[1 / F \left(\frac{\xi_i}{2\sqrt{D_{Al}t}} \right) \right] \tag{3}$$

where ξ_i is the distance of the internal precipitation front from the original alloy surface, ξ_c the position of the scale/alloy interface with respect to the original surface, N_{Al}^O the mole fraction of Al in the bulk alloy and $F(u)$ the auxiliary function in the form of $F(u) = \pi^{1/2} u \exp(u^2) \operatorname{erfc}(u)$. In the case of internal oxidation considered here, u is related to N_o^S , D_o , D_{Al} and N_{Al}^O .

Figure 5 shows cross-sectional images of the model alloy 2 (Ni-4.6Cr-2.4Al) after 20 h oxidation in the two different environments at 1,000 °C. Four interfaces,

which are labeled as 1–4 in Fig. 5b, can be identified in the two images. Interface 1 is the scale surface. Interface 2 is considered to be the original alloy surface because internal oxidation precipitates, which started from this interface, served as intrinsic markers. Interface 3 is between the external scale and the alloy and interface 4 is at the maximum depth of internal oxide formation. From interface 1 to 3, NiO was the main phase, as determined on the basis of compositional analysis using EDS. The region between interfaces 2 and 3 is the metal-consumption zone (MCZ), which formed as a consequence of Ni being selectively oxidized to form NiO. Since part of the IOZ was incorporated into the MCZ, the total thickness of the former (ξ_i) was equated to be the combination of the MCZ and the subsurface precipitate zone (interface 3–4). The average ξ_i was found to be around 66 μm ($\pm 4 \mu\text{m}$) in dry air and 69 μm ($\pm 4 \mu\text{m}$) in wet air. Meanwhile, ξ_c was found to be around 9 μm ($\pm 2 \mu\text{m}$) in dry air and 29 μm ($\pm 2 \mu\text{m}$) in wet air. The diffusion coefficient of aluminum in the alloy (D_{Al}) has been reported in several papers [27–29] and an accurate temperature dependence is deduced to be:

$$D_{Al} = 1.0 \exp\left(\frac{-260\text{kJ/mol}}{RT}\right) \text{cm}^2/\text{sec}. \quad (4)$$

Thus, at 1,000 °C, D_{Al} is $2.1 \times 10^{-11} \text{cm}^2/\text{sec}$. This parameter was assumed to be the same in both oxidizing conditions. Another important parameter that is needed to accurately assess the results using Eq. 3 is the stoichiometry factor v . Since there are two types of internal oxides, NiAl_2O_4 and Al_2O_3 , this factor should be replaced by an effective stoichiometry factor v_{eff} , which depends on the ratio of the distances for the two internal oxidation fronts (for forming NiAl_2O_4 and Al_2O_3) and the corresponding oxygen potentials at those two internal oxidation fronts [30]. From Fig. 5, these two phases can be clearly identified by their contrast. The dash lines show the position where Al_2O_3 (black precipitates) starts to form. It is seen that the distances for the two internal oxidation fronts in the two conditions were not significantly changed. Therefore, the v_{eff} was considered to be unchanged by the presence of steam. Substituting D_{Al} , ξ_i and ξ_c for the two conditions into Eq. 3, the oxygen permeability is found to decrease by around 25 % when 30 % steam is introduced into the atmosphere. Comparable results were found at both shorter and

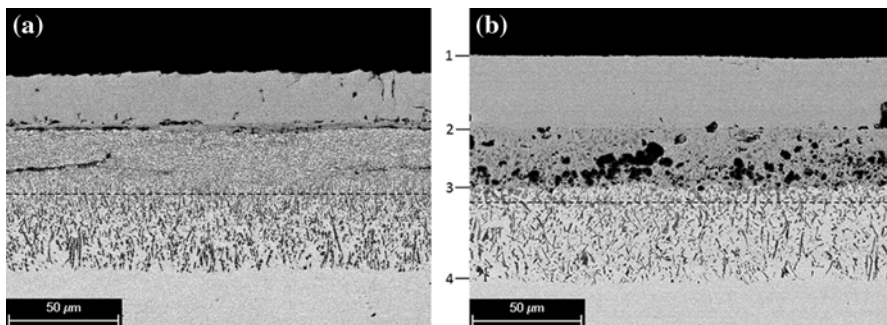


Fig. 5 Cross-sectional images of Ni-4.6Cr-2.4Al (wt%) after being oxidized in dry (a) and wet (b) air at 1,000 °C for 20 h

longer oxidation times. Interestingly, and for reasons that are currently not clear, Setiawan et al. [31], reported a $\sim 20\%$ increase in the oxygen permeability of zFe–Cr alloys when exposed to a steam-containing atmosphere at 700 and 800 °C.

To assess the effect of any change in oxygen permeability on N_{Al}^* , it is worth noting that Eq. 2 is valid only under a limiting case, which requires:

$$\frac{N_o^S}{N_{Al}^O} \ll \frac{D_{Al}}{D_o} \ll 1. \quad (5)$$

From this requirement, $N_o^S D_o$ needs to be much smaller than $N_{Al}^O D_{Al}$. From previous study [24], D_o and N_o^S values at 1,000 °C were found to be 1.0×10^{-7} cm²/sec and 5.4×10^{-4} , respectively. The N_{Al}^O value is approximated to be 0.3. Multiplying N_o^S by D_o and N_{Al}^O by D_{Al} yields $N_o^S D_o \gg N_{Al}^O D_{Al}$, indicating that the requirement stipulated by Eq. 5 was not met for Ni–Al alloy oxidized at 1,000 °C. Therefore, for Ni–Al systems oxidized at this temperature, N_{Al}^* is not directly related to the oxygen permeability, as suggested by Eq. 2. Alternatively, the effect of changing the oxygen permeability can be assessed by determining the enrichment factor α . This is done in the following.

Darken [32] recognized that the volume fraction of internal oxide precipitates would affect the critical concentration. Wagner [14] proposed that the external scale formation is favored when the volume fraction of the internal oxide precipitates (f_v) reaches some critical value (f_v^*). Converting the volume fraction (f_v) to mole fraction (f) yields:

$$f_v = \frac{f \cdot V_{AlO_v}}{V_{all}} \quad (6)$$

where V_{AlO_v} is the equivalent molar volume of AlO_v . Further, f is determined by the mole fraction of Al in the alloy (N_{Al}^O), and whether Al is enriched in the IOZ by a supply of Al from the alloy bulk. Such enrichment can be defined as [14]:

$$\alpha = \frac{f}{N_{Al}^O}. \quad (7)$$

When there is no Al enrichment in the IOZ, i.e., α equals unity, the mole fraction of AlO_v in the IOZ is the same as the mole fraction of Al in the alloy.

Substituting Eqs. 6 and 7 into the criterion $f_v \geq f_v^*$, gives:

$$N_{Al}^* = \frac{f_v^* \cdot V_{all}}{\alpha \cdot V_{AlO_v}}. \quad (8)$$

In this equation, V_{AlO_v} and V_{all} can be considered as two constants. Therefore, N_{Al}^* is sensitive to any change in α and f_v^* . If for any reason α is changed by the presence of steam, the N_{Al}^* value will correspondingly change. Moreover, it can be shown that α is related in a complex way to the auxiliary function [14]. As a consequence, a change in the oxygen permeability may influence the value of N_{Al}^* by influencing the value of α . To assess this it is necessary to determine if α differed for the two oxidizing conditions studied even though the oxygen permeabilities did differ.

Figure 6 shows cross-sectional images of the bottom region of the IOZ in model alloy 2 oxidized in dry and wet air at 1,000 °C for 20 h. It was found from

quantitative analysis of corresponding digitized images (Fig. 6c, d) that the area fraction of internal precipitates formed in the dry oxidizing condition is 30 % (± 2 %), which is almost identical to the measurement of 29 % (± 2 %) for the wet oxidizing condition. Since these fractions are based on a two-dimensional area measurement, they need to be converted to volume fractions. In accordance with the principles of quantitative microscopy [33], if the selection of cross-sectional images is completely random, then the average area fraction of a cross-sectional image should be the same as the volume fraction, i.e.,

$$\overline{A_A} = f_v \quad (9)$$

where $\overline{A_A}$ is the average area fraction of precipitates. Since the cross-sectional images in Figs. 6c and d contain a large amount of precipitates and images taken at different positions on the same sample showed that the area fractions are statistically at the same level (± 2 %), Eq. 9 is inferred to be valid for the present analysis. Therefore, the similar $\overline{A_A}$ in the two oxidizing conditions indicates that f_v is the same. Based on Eq. 6, f does not change either. Since N_{Al}^O is a constant for a given alloy, the enrichment is then the same by its definition, i.e., Eq. 7. Therefore, although there was a 25 % decrease in the oxygen permeability, it did not change α . This means that the observed change in N_{Al}^* for the two conditions cannot be attributed to the 25 % difference measured in the oxygen permeabilities. Therefore, the only parameter in Eq. 8 that can give the large increase in N_{Al}^* is the f_v^* .

Upon closer inspection of the images in Fig. 6 it becomes clear that the morphology of the internal oxide precipitates is different for the dry and wet oxidizing conditions. This morphology change can be quantified by drawing a line of a fixed length across an IOZ image and counting the number of precipitates that

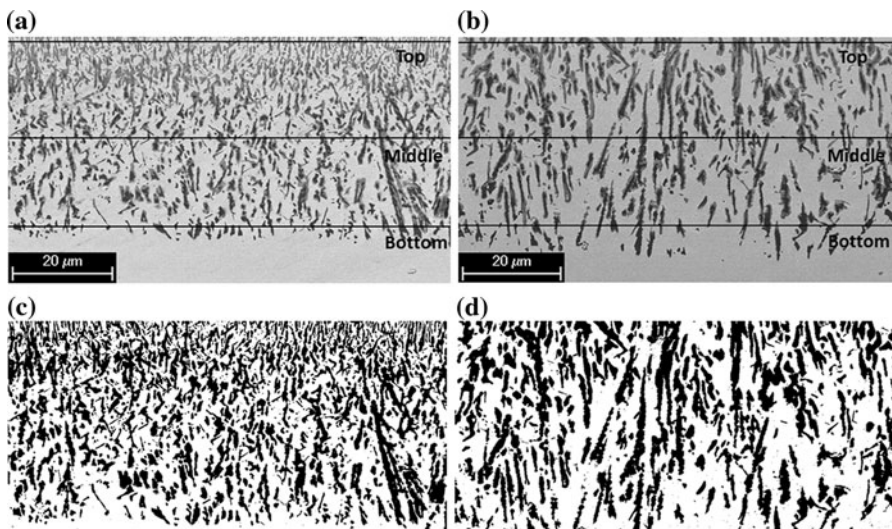


Fig. 6 The morphology of the internal oxides formed on Ni-4.6Cr-2.4Al alloy oxidized in **a** dry air and **b** air + 30 %H₂O at 1,000 °C for 20 h

Table 2 Number of internal precipitates on a line going from the left to the right of the cross-sectional image of Ni-4.6Cr-2.4Al oxidized in dry air and air + 30 %H₂O at 1,000 °C for 20 h

Number	Top	Middle	Bottom
Dry air	110 ± 20	70 ± 16	39 ± 14
Air + 30 %H ₂ O	40 ± 10	32 ± 9	21 ± 9

intersect with that line (i.e., lineal analysis). Table 2 shows the average number of precipitates for the three lines shown in Figs. 6a and b. Similar measurements were made on at least three different images. The numbers in Table 2 reveal that, for a given exposure period, much fewer precipitates formed in the alloy oxidized in wet air. Given that the volume fraction of the precipitates is the same, the sizes of the precipitates must be larger and the distance between them greater when steam is present. The reason that the morphology and distribution was changed by the presence of steam is not clear, though it seems likely that hydrogen is playing a role. For instance, hydrogen may change the diffusion path and therefore the driving force for nucleation of precipitates. Regardless of the mechanism involved, it is easy to rationalize that if the distances between the internal oxidation precipitates are increased by the presence of steam, the establishment of a continuous layer by lateral growth of those internal oxidation precipitates would be made more difficult. Thus, based on this analysis, it is deduced that the critical volume fraction f_v^* in Eq. 8 is increased for the wet oxidizing condition tested in this study. Although this factor is usually assumed to be a constant 0.3 and independent of the reacting conditions [34], there exists no clear elucidation of this factor. In fact, it is suggested based on this analysis that number density and, hence, interparticle spacing must also be considered in conjunction with volume fraction.

Conclusions

The effects of 30 % steam on the oxidation behavior of Al₂O₃-scale forming Ni-based alloys were studied. It was found that the commercial alloy AM1 became less protective in the steam-containing environment, while another commercial alloy Rene N5 remained protective. To study this steam effect on N_{Al}^* for Al₂O₃-scale forming Ni-based alloys, a pair of Ni–Cr–Al model alloys were further investigated. It was found that Ni-9.2Cr-2.4Al is protective when oxidizing in dry air at 1,000 °C. However, it becomes less protective, i.e., forming NiO scale and internal Al₂O₃ when oxidizing in wet air at the same temperature. This comparison showed that N_{Al}^* is increased when steam is present. Early stage (5 min and 30 min of reaction) oxidation of this alloy in the two atmospheres showed that the oxidation behavior was different from the very beginning of reaction, which means Wagner's criterion for sustaining the growth of an existing Al₂O₃ scale was not applicable for assessing the change in the N_{Al}^* under the conditions studied.

By Maak's equation for oxygen permeability for the case of internal oxidation coupled with external scale formation and a study of internal oxidation in a dilute

model alloy of composition Ni-4.6Cr-2.4Al, it was found that the oxygen permeability into the alloy was decreased by around 25 % the presence of steam. From quantitative image analysis, it was found that the enrichment factor α remained the same in dry and wet oxidizing conditions. Therefore, based on an equation derived from Wagner's criterion for transition from internal oxidation to external scale formation (Eq. 8), it was deduced that the only factor that can change the critical concentration N_{Al}^* is the critical volume fraction f_v^* . By comparing the morphology of the internal oxides formed in the two oxidizing conditions, it was found that the internal-oxide precipitates are coarser and their average spacing is greater in the wet oxidizing condition. This is true even though the volume fraction of internal oxide was unaffected by the presence of steam. Therefore, more precipitates are required to reduce the spacing between precipitates which, in turn, means that f_v^* must be increased for a steam-containing atmosphere. This means that f_v^* is not fixed, as it is usually assumed to be, but is instead a variable that is dependent on the oxidizing condition.

Acknowledgments This research is supported by the U.S. Office of Naval Research, award N000014-09-1-1127 and managed by Dr. David Shifler.

References

1. F. S. Pettit, *Transactions of the metallurgical society of AIME* **239**, 1296 (1967).
2. C. S. Giggins and F. S. Pettit, *Journal of the Electrochemical Society* **118**, 1782 (1971).
3. I. A. Kvernes and P. Kofstad, *Metallurgical Transactions* **3**, 1511 (1972).
4. M. C. Maris-Sida, G. H. Meier and F. S. Pettit, *Metallurgical and Materials Transactions A* **34A**, 2609 (2003).
5. R. Janakiraman, G. H. Meier and F. S. Pettit, *Metallurgical and Materials Transactions A* **30A**, 2905 (1999).
6. F. A. Elrefaie, A. Manolescu and W. W. Smeltzer, *Journal of the Electrochemical Society* **132**, 2489 (1985).
7. H. C. Yi, S. W. Guan, W. W. Smeltzer and A. Petric, *Acta Metallurgica et Materialia* **42**, 981 (1994).
8. J. A. Nesbitt, *Journal of the Electrochemical Society* **136**, 1511 (1989).
9. J. A. Nesbitt, *Journal of the Electrochemical Society* **136**, 1518 (1989).
10. F. Gesmundo and F. Viani, *Oxidation of Metals* **25**, 269 (1986).
11. F. Gesmundo, F. Viani and Y. Niu, *Oxidation of Metals* **42**, 285 (1994).
12. Y. Niu and F. Gesmundo, *Oxidation of Metals* **65**, 329 (2006).
13. S. Wang, F. Gesmundo and Y. Niu, *Oxidation of Metals* **72**, 279 (2009).
14. C. Wagner, *Z. Elektrochem* **63**, 772 (1959).
15. C. Wagner, *Journal of the Electrochemical Society* **103**, 571 (1956).
16. M. A. Alvin, Department of Energy, National Energy Technology Laboratory, Pittsburgh, OA, USA (private communication).
17. E. Essuman, G. H. Meier, J. Zurek, M. Hansel and W. J. Quadackers, *Oxidation of Metals* **69**, 143 (2008).
18. J. Zurek, M. Michalik, F. Schmitz, T.-U. Kern, L. Singheiser and W. J. Quadackers, *Oxidation of Metals* **63**, 401 (2005).
19. S. Hayashi and T. Narita, *Oxidation of Metals* **56**, 251 (2001).
20. A. Rahmel and T. Tobolski, *Corrosion Science* **5**, 333 (1965).
21. J. Ehlers, D. J. Young, E. J. Smaardijk, A. K. Tyagi, H. J. Penkella, L. Singheiser and W. J. Quadackers, *Corrosion Science* **48**, 3428 (2006).
22. A. Galerie, S. Henry, Y. Wouters, M. Mermoux, J. P. Petit and L. Anton, *Materials at High Temperatures* **22**, 105 (2005).
23. Y. Ikeda and K. Nii, *Transactions of National Research Institute for Metals* **26**, 52 (1984).

24. W. Zhao, Ph.D thesis, University of Pittsburgh, 2012.
25. R. A. Rapp, *Corrosion*. **21**, 382 (1965).
26. F. Maak, *Z. Metallkde* **52**, 545 (1961).
27. W. Gust, H. B. Hintz, A. Lodding, H. Odellius and B. Predel, *Physica Status Solidi* **64**, 187 (1981).
28. A. Green and N. Swindells, *Materials Science and Technology* **1**, 101 (1985).
29. M. M. P. Janssen, *Metallurgical Transactions* **4**, 1623 (1973).
30. J. L. Meijering, *Advanced Materials Research* **5**, 81 (1971).
31. A. R. Setiawan, M. H. B. Ani, M. Ueda, K. Kawamura and T. Maruyama, *ISIJ International* **50**, 259 (2010).
32. L. S. Draken, *Transactions. AIME*. **150**, 157 (1942).
33. R. T. DeHoff and F. N. Rhines, in *Quantitative Microscopy*, (Mcgraw-Hill, New York, 1991), p. 46.
34. R. A. Rapp, *Acta. Metallurgica*. **9**, 730 (1961).